Check for updates

Effect of additives, ball milling and isotopic exchange in porous magnesium borohydride†

Michael Heere, [ID] *[ab] Olena Zavorotynska,[ac] Stefano Deledda,[a] Magnus H. Sørby,[a] David Book,[d] Theodore Steriotis[e] and Bjørn C. Hauback[a]

Magnesium borohydride ($Mg(BH_4)_2$) is a promising material for solid state hydrogen storage. However, the predicted reversible hydrogen sorption properties at moderate temperatures have not been reached due to sluggish hydrogen sorption kinetics. Hydrogen (H) → deuterium (D) exchange experiments can contribute to the understanding of the stability of the BH_4^- anion. Pure γ-$Mg(BH_4)_2$, ball milled $Mg(BH_4)_2$ and composites with the additives nickel triboride (Ni_3B) and diniobium pentaoxide (Nb_2O_5) have been investigated. *In situ* Raman analysis demonstrated that in pure γ-$Mg(BH_4)_2$ the isotopic exchange reaction during continuous heating started at ~80 °C, while the ball milled sample did not show any exchange at 3 bar D_2. However, during *ex situ* exchange reactions investigated by infrared (IR) and thermogravimetric (TG) analyses a comparable H → D exchange during long exposures (23 h) to deuterium atmosphere was observed for as received, ball milled and γ-$Mg(BH_4)_2$ + Nb_2O_5, while the Ni_3B additive hindered isotopic exchange. The specific surface areas (SSA) were shown to be very different for as received γ-$Mg(BH_4)_2$, BET area = 900 m^2 g^{-1}, and ball milled $Mg(BH_4)_2$, BET area = 30 m^2 g^{-1}, respectively, and this explains why no gas−solid H(D) diffusion was observed for the ball milled (amorphous) $Mg(BH_4)_2$ during the short time frames of *in situ* Raman measurements. The heat treated ball milled sample partially regained the porous γ-$Mg(BH_4)_2$ structure (BET area = 560 m^2 g^{-1}). This in combination with the long reaction times allowing for the reaction to approach equilibrium explains the observed gas−solid H(D) diffusion during long exposure. We have also demonstrated that a small amount of D can be substituted in both high surface area and low surface area samples at room temperature proving that the B−H bonds in $Mg(BH_4)_2$ can be challenged at these mild conditions.

Introduction

Research on solid state hydrogen storage materials has been enormously extended in the last 20 years, ever since Bogdanović and Schwickardi reported reversible hydrogenation in Ti-catalyzed sodium alanate, $NaAlH_4$.[1] Many compounds have been considered for hydrogen storage applications and magnesium borohydride, $Mg(BH_4)_2$, is still one of the most promising candidates, with a high hydrogen content (14.9 wt% H) and predicted reversible hydrogen sorption properties at

aDepartment for Neutron Materials Characterization, Institute for Energy Technology, NO-2027 Kjeller, Norway

bInstitute for Applied Materials – Energy Storage Systems (IAM – ESS), Karlsruhe Institute of Technology (KIT), D–76344, Eggenstein-Leopoldshafen, Germany. E-mail: michael.heere@kit.edu

cInstitute for Mathematics and Physics, University of Stavanger, PO Box 8600 Forus, NO-4036 Stavanger, Norway

dSchool of Metallurgy and Materials, University of Birmingham, Birmingham B15 2TT, UK

eInstitute of Nanoscience and Nanotechnology, NCSR "Demokritos", Ag. Paraskevi Attikis, Athens 15341, Greece

† Electronic supplementary information (ESI) available. See DOI: 10.1039/c8ra05146a

moderate temperatures.[2,3] The compound is potentially suitable for the operating temperature window of polymer electrolyte membrane (PEM) fuel cells (~80 °C). The synthesis of $Mg(BH_4)_2$ from hydrogenation of MgB_2 was first achieved at 400 °C and 900 bar hydrogen.[4] Furthermore, decomposition of $Mg(BH_4)_2$ at moderate temperatures (~200 °C) resulted in the formation of $Mg(B_3H_8)_2$, which can almost completely be rehydrogenated to $Mg(BH_4)_2$ within 48 h at 250 °C and 120 bar H_2,[5] and thus reversibly cycling 2.5 wt% H. Nevertheless, Zavorotynska *et al.* reported similar results on a much shorter time scale.[6] 2.5 wt% hydrogen were reabsorbed at 260 °C under 120 bar H_2 in 7–8 h, and the reaction was completed in less than 3 h at 280 °C.

Efforts in tailoring the hydrogen storage properties of $Mg(BH_4)_2$ have been continuing. Addition of small amounts of various transition-metal compounds, with the goal to improve kinetics and reversibility of hydrogen desorption in $Mg(BH_4)_2$, has been a subject of several recent studies. Transition-metal (TM) oxides, chlorides or fluorides, with TM = Sc, Ti, V, Co, Ni, Zn, Nb, Mo, Ru and Pd[7−17] have been employed and showed improvement of hydrogen release during the first desorption.[18] Saldan *et al.*[18] investigated the effect of various Ni-based additives in $Mg(BH_4)_2$ and reported that NiF_2 and $NiCl_2$

transformed into a phase "resembling Ni₃B" after the first hydrogen desorption. Therefore, Ni₃B appeared to be the most promising candidate to improve the hydrogen release properties of $Mg(BH_4)_2$. $Mg(BH_4)_2$ including 2 mol% Ni₃B has shown a release of 2.7 wt% H during a 15 h desorption measurement at 220 °C under static vacuum,[18] whereas it took 800 h at 200 °C to desorb the same amount from pure $Mg(BH_4)_2$.[5]

$Mg(BH_4)_2$ has a rather unique crystal chemistry.[19] In total, there are currently seven known polymorphs: α-, β-, γ-, δ- and ζ-$Mg(BH_4)_2$ have been structurally characterized,[20–23] two yet unsolved structures ε- and β′-$Mg(BH_4)_2$,[24,25] and an unidentified structure was recently proposed.[19] Furthermore, non-crystalline amorphous $Mg(BH_4)_2$ has been obtained from solvent-free synthesis,[26] by ball milling of the crystalline α- and γ-phases[22] and *via* pressure collapse of γ-$Mg(BH_4)_2$.[27] γ-$Mg(BH_4)_2$ exhibits a characteristic porous structure, and its specific surface area (SSA) of 1160 m² g⁻¹ is the highest so far found in complex hydrides.[22] It is higher than the SSA of high performing organosilicas[28,29] and can be compared to the SSA of metal organic frameworks (MOFs). It has been shown that it is possible to reversibly adsorb N₂, CH₂Cl₂ and even 3 wt% of hydrogen (at 83 K, 105 bar) in γ-$Mg(BH_4)_2$.[22] Possible thermal decomposition pathways of different polymorphs of $Mg(BH_4)_2$ are reviewed by Zavorotynska *et al.*[19]

Isotopic experiments in group I and II metal borohydrides have been carried out by different research groups.[30] Recently, Zavorotynska *et al.*[31] demonstrated the H → D isotopic exchange reaction in porous γ-$Mg(BH_4)_2$ at much milder conditions than reported for isotopic exchange in the denser α-$Mg(BH_4)_2$ phase.[32] In α-$Mg(BH_4)_2$, the isotopic exchange reaction was observed at 132 °C after prolonged treatment at 42 bar D₂, whereas the exchange in porous γ-$Mg(BH_4)_2$ was recorded after ~17 min at 100 °C under only 3 bar D₂. The authors concluded that the porous nature and resulting high specific surface area of γ-$Mg(BH_4)_2$ was responsible for the rapid exchange reaction occurring at the surface at mild conditions.

In this work, isotopic exchange is used to obtain a deeper understanding of the effect of additives and/or ball milling, on the hydrogen sorption kinetics of γ-$Mg(BH_4)_2$. Firstly, we have compared the H₂ release in as received and ball milled γ-$Mg(BH_4)_2$ as well as γ-$Mg(BH_4)_2$ milled with Nb- and Ni-based additives (2 mol%). Nb₂O₅, to the best of our knowledge, has not been explored for improving the properties of $Mg(BH_4)_2$, but has been reported to enhance kinetics in hydrogen desorption and absorption in MgH₂.[33] Secondly, we have shown the influence of additives and/or ball milling on the H → D isotopic

exchange in γ-$Mg(BH_4)_2$. The isotopic exchange reactions were studied by thermogravimetric and differential scanning calorimetry (TG-DSC), infrared (IR) and *in situ* Raman measurements. Furthermore, synchrotron radiation powder X-ray diffraction (SR-PXD) measurements, including *in situ* SR-PXD, were carried out for all samples. Nitrogen adsorption isotherms were measured at 77 K for the as received, the ball milled $Mg(BH_4)_2$ as well as their heat treated analogues in order to determine their specific surface area.

Experimental details

γ-$Mg(BH_4)_2$ (95%) and Nb₂O₅ (99%) were purchased from Sigma Aldrich and used without further purification. The additive Ni₃B was prepared as described in ref. 18.

All sample manipulations were carried out under inert conditions. An MBraun glove box fitted with a recirculation system was used with oxygen and humidity levels kept below 1 ppm during all operations. Mechanochemical milling (ball milling, bm) with and without 2 mol% additives was carried out using a Fritsch Pulverisette 6 planetary mill. Steel vial and balls were used and a ball-to-powder ratio of 40 : 1 was employed. The powders were milled for 4 × 15 min at 300 rpm with breaks of 5 min to avoid overheating. The synthesis procedures of the four investigated samples, S1–S4, are summarized in Table 1.

Thermogravimetric and differential scanning calorimetry (TG-DSC) experiments were conducted using a Netzsch STA 449 F3 Jupiter analyser. Two sets of experiments were conducted. The first set was measured from room temperature (RT) to 285 °C at 5 °C min⁻¹. The second set of experiments were carried out by heating from RT to 450 °C at heating rates of 1, 2, 5 and 7 °C min⁻¹, respectively. All measurements were conducted within Al crucibles. The Ar flow (protective and purge gas) was 20 and 50 ml min⁻¹, respectively. The peak search function in the Netzsch software (proteus thermal analysis) was used to determine peak temperatures in the DSC data. For overlapping events, the peak shape fitting function in the software Fityk[34] was employed, with a Gaussian function, in which parameters such as peak height, position, half width at half maximum and shape were fitted one by one (ESI Fig. A1†). Temperature programmed desorption-mass spectrometry (TPD-MS) was performed in an in-house manufactured apparatus connected to a MKS Microvision-IP Residual Gas Analyser. The powder (~10 mg) was loaded in a steel sample holder and heated from RT to 400 °C with a heating rate of 5 °C min⁻¹ under dynamic vacuum.

Table 1 Compositions and synthesis procedures of the investigated samples. Molar weight (M), nominal H-content and average weight loss (Δ*m*) of independent TG-DSC measurements are presented as well as the H loss in percent of the total hydrogen content calculated from ΔTG data (decomposition from RT to 450 °C)

Sample name	Composition	Procedure	M (g mol⁻¹)	H-content (wt%)	Δ*m* (wt%)	H loss (%)	Sample name after 23 h H → D exchange at 120 °C
S1	γ-$Mg(BH_4)_2$	As received	53.99	14.94	13.5 ± 0.3	90 ± 2	S1-D
S2	γ-$Mg(BH_4)_2$	Ball milling	53.99	14.94	13.1 ± 0.3	87 ± 2	S2-D
S3	γ-$Mg(BH_4)_2$ + 2 mol% Ni₃B	Ball milling	57.73	13.97	12.3 ± 0.1	88 ± 1	S3-D
S4	γ-$Mg(BH_4)_2$ + 2 mol% Nb₂O₅	Ball milling	59.31	13.60	11.8 ± 0.5	86 ± 3	S4-D

The deuterium exchange experiments were executed in an in-house manufactured Sieverts type apparatus[35] at 3 bar D_2 and 120 °C. During all experiments the furnace was preheated to 120 °C before the steel autoclave with the sample was introduced. The D_2 pressure was adjusted to 3 ± 0.05 bar at RT and did not rise significantly during heating due to the large volume of the Sieverts apparatus. The duration of the exchange reaction at 120 °C was chosen to 23 h. Samples were contained in sealed Al-crucibles with a pierced lid, which were placed inside an in-house manufactured steel autoclave. For H → D exchange at elevated temperature, the samples S1–S4 were treated individually. TG data were employed to calculate the deuterium content (ESI Fig. A2†).

Synchrotron radiation powder X-ray diffraction (SR-PXD) data were collected at the Swiss Norwegian Beam Line (SNBL), BM01 at the European Synchrotron Radiation Facility (ESRF), Grenoble, France. For SR-PXD experiments at RT the samples were contained in 0.5 mm sealed boron glass capillaries. For *in situ* SR-PXD experiments, sapphire capillaries with 1.2 mm and 0.8 mm outer and inner diameter, respectively, were connected *via* Vespel ferrules to an in-house manufactured remote controlled gas rig and high pressure manifold cell. The sample-to-detector distances and the wavelength were calibrated from a NIST LaB_6 standard. Data were collected using a Pilatus 2M detector. The exposure time was set to 30 s giving a temperature resolution of 2.5 °C per pattern and the sapphire capillary was rotated by 10° during exposure to improve powder averaging. Single crystal reflections from the sapphire tube were masked manually and the data were integrated to 1D diffraction patterns in Fit2D and Bubble.[36,37]

Attenuated total reflection IR (ATR-IR) measurements were performed using a Bruker Alpha-Platinum infrared spectrometer with a diamond crystal inside an Ar-filled glove box. The spectra were obtained in the wavenumber range of 4000–400 cm^{-1} with a resolution of 2 cm^{-1} at RT. Three measurements each including 32 scans were averaged for each spectrum and the background. IR spectra were ATR corrected and normalized using commercial spectroscopic software OPUS. The samples were measured without any dilution.

In situ Raman spectra were measured employing a Renishaw inVia Raman microscope with a 488 nm excitation laser (usually 2 mW on the sample). To focus the laser beam onto the sample a microscope objective with a spot diameter of 50 μm was used. An Instec sample HCS621 V cell with a fused silica window was employed for H → D exchange measurements at 3 bar D_2 pressure while heating was conducted in this cell between RT and 175 °C at 2 °C min^{-1}. The cell was flushed with argon before use. Each scan consists of 10 times 5 s data acquisition, with automatic refocusing after every fifth scan. The temperature resolution was 1.7 °C per pattern. Data processing with the software WiRe 4.0 included baseline correction and cosmic ray removal, as well as normalization for samples S1 and S2. Furthermore, the data was smoothed, with special emphasis that no peaks were removed during smoothing.

N_2 adsorption isotherms were carried out at −196 °C (77 K) on an Autosorb-1MP volumetric analyzer equipped with a Gifford-McMahon cryocooler, which is a two-stage closed cycle

refrigeration unit (CCR) working from −265 °C to +47 °C (8–320 K). The samples were outgassed at 35 °C under high vacuum (<10^{-6} mbar), usually for 8–10 h. Preliminary N_2 adsorption measurements of the as received S1 at −196 °C (77 K) revealed extremely poor kinetics. For this reason very strict equilibration criteria (pressure change <0.00001 bar h^{-1}) were used for S1 and S2, leading to equilibration times of several hours per point. Due to the ultra-microporous character of some samples low relative pressure measurements ($p/p_0 = 10^{-6}$ – 0.995) were employed. Similar measurements were carried out on the heat treated S1 and S2 samples. The heat treated samples were named S1-H and S2-H in analogy to S1-D and S2-D (Table 1) as the same conditions (120 °C and 3 bar H_2 for 23 h) were used, but with hydrogen instead of deuterium. In all cases BET areas were calculated by taking into consideration the pertinent IUPAC consistency criteria for microporous materials. Alternative models for area determination such as Langmuir, Dubinin–Radushkevich (DR) and micropore analysis method (MP-method) were applied as well to validate the data.[38–40] Total pore volumes were calculated from the plateau region by assuming liquid N_2 density in the pores.

Results and discussion

Effect of additives *vs.* ball milling

The SR-PXD data at RT for samples S1–S4 are presented in Fig. 1. For S1 only Bragg peaks of γ-$Mg(BH_4)_2$ are observed on a low background.[22] However, the ball milled S2 and S3 show strong diffuse scattering and only traces of Bragg peaks from γ-$Mg(BH_4)_2$, indicating almost complete amorphization during the milling process.[22] Bragg peaks of the Ni_3B additives could not be observed in S3, which is due to its amorphous nature and in agreement with previous work.[18] In S4 diffuse scattering is present as well, but with more intense Bragg peaks of the γ-
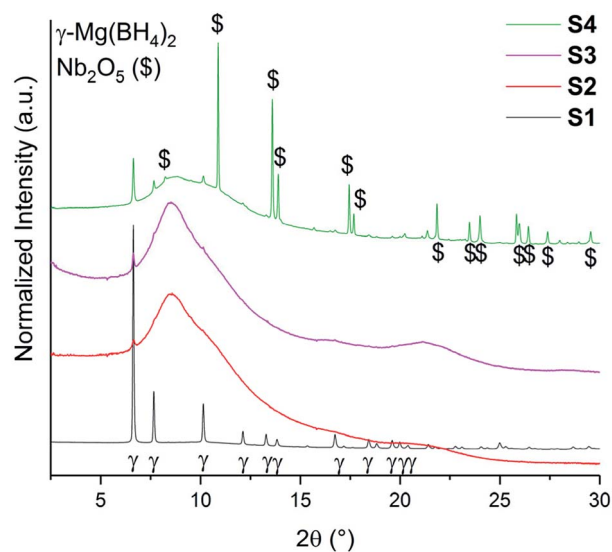

Fig. 1 SR-PXD data of γ-$Mg(BH_4)_2$ samples (S1–S4) at RT. All samples have been normalized to its maximum intensity and are shifted on the *y*-axis for better visibility. λ = 0.7454 Å.

$Mg(BH_4)_2$ phase compared to S2.[18] Bragg peaks of Nb_2O_5 are identified for S4. No contaminations have been found in S1–S4. The first order phase transitions of γ-$Mg(BH_4)_2$ to ε-$Mg(BH_4)_2$ (ref. 25) and from ε- into β'-$Mg(BH_4)_2$ (ref. 24) have previously been reported. *In situ* SR-PXD measurements were employed in order to study how additives influence the phase transitions in crystalline $Mg(BH_4)_2$. Fig. 2a shows *in situ* SR-PXD data of S4 heated from RT to 285 °C at 5 °C min^{-1} followed by a 1 h isotherm, while Fig. 2b is presenting the same SR-PXD data at selected temperatures for a better visualization. For clarity the data are only given up to $2\theta = 10°$, and thus excluding most Bragg peaks of Nb_2O_5. 285 °C was chosen as the end temperature because earlier reports suggested melting and/or formation of amorphous phases above 285 °C,[14] followed by the formation of very stable $B_{12}H_{12}$ phases at higher temperatures.[4] Bragg peaks of γ-$Mg(BH_4)_2$ and Nb_2O_5 are present at RT. Upon heating, Bragg peaks of γ-$Mg(BH_4)_2$ sharpen until 142 °C (red curve in Fig. 2b). A crystallization reaction is the probable cause for peak sharpening, corresponding to an increase in crystallinity. Upon further heating the Bragg peaks of γ-$Mg(BH_4)_2$ decrease in intensity and vanish at 173 °C. Bragg peaks corresponding to ε-$Mg(BH_4)_2$ (ref. 25) appear at 154 °C and have their highest

intensity at 178 °C (Fig. 2b, blue curve). ε-$Mg(BH_4)_2$ is transformed directly into β'-$Mg(BH_4)_2$,[24] appearing at 197 °C and the highest intensity is observed at 248 °C (magenta curve). The disappearance of Bragg peaks after 18 min in the 285 °C isotherm has been reported before and is due to formation of an amorphous phase and possibly a reversible product which is very likely $Mg(B_3H_8)_2$.[13] In the isothermal regime no further reactions occur. The *in situ* SR-PXD data of S3 (ESI Fig. A4†) show Bragg peaks of γ-$Mg(BH_4)_2$ which appear between RT and $\sim$150 °C. Bragg peaks of β'-$Mg(BH_4)_2$ are observed between 195 and 285 °C, while ε-$Mg(BH_4)_2$ is not observed.

TG-DSC data of S1–S4 heated from RT to 285 °C (5 °C min^{-1}) are presented in Fig. 3. The first exothermic peak in the DSC data of S2 and S4 at 100 °C and of S3 at 120 °C stems from the crystallization of amorphous into γ-$Mg(BH_4)_2$. For S3 an elevated baseline and increased temperature of crystallization was observed. However, for S1 the first order transitions from γ-phase into ε-$Mg(BH_4)_2$ ($T_{onset} = 153$ °C) and from ε- into β'-$Mg(BH_4)_2$ ($T_{onset} = 185$ °C) can be clearly observed. Notably, they are shifted to slightly lower temperatures for the other samples. The onset temperatures of phase transitions for S2–S4 are very similar, 150 °C and 177 °C, respectively. These observations suggest a decreased stability of γ-phase in S2–S4, which is likely to have been induced by ball milling. The TG data between RT and 285 °C show that all samples have fairly similar weight loss (3.7 wt%), when considering that TG data are not corrected for the amounts of the additives (raw data in Fig. 3).

The decomposition of γ-$Mg(BH_4)_2$ can be divided into four steps, all taking place above 285 °C. TG-DSC data between RT and 450 °C are shown in ESI Fig. A3a–d.† A new fifth decomposition step is present in S2 and S4, and has not been assigned yet. It is an endothermic event and thus a decomposition of an intermediate Mg–B–H species is likely.[41] Nevertheless, all decomposition events are possibly accompanied by the formation of intermediate Mg–B–H species including higher boranes.[42] The decomposition of S1–S4 have been investigated by four TG-DSC measurements at different heating rates (1, 2, 5,
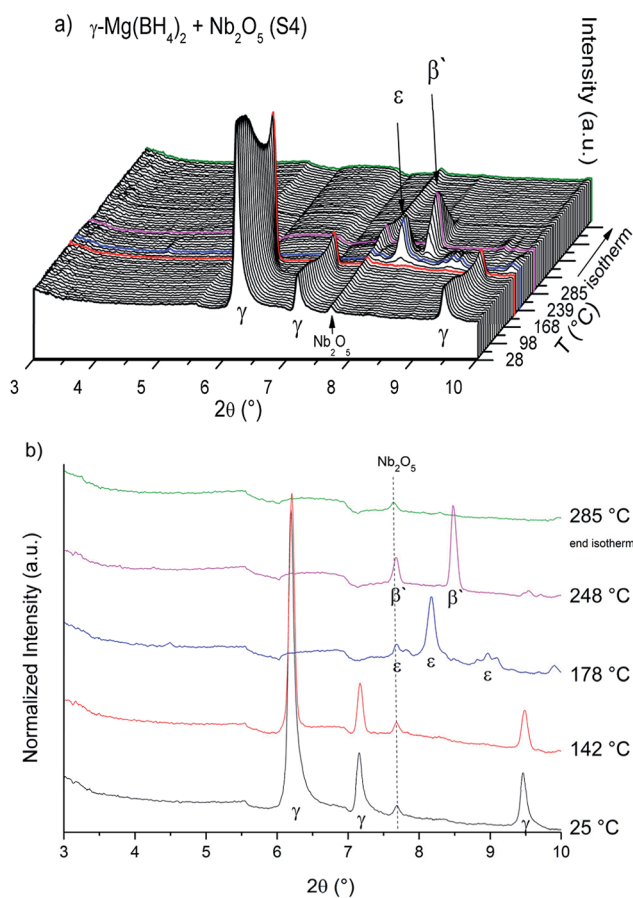

Fig. 2 (a) *In situ* SR-PXD data of ball milled $Mg(BH_4)_2$ + Nb_2O_5 (S4) heated from RT to 285 °C under 2.3 bar H_2 (temperature ramp of 5 °C min^{-1}) and 1 h isotherm. (b) SR-PXD data of S4 at specific temperatures. Curves in different colours are used from (a) for better visualization. $\lambda = 0.6973$. Å.
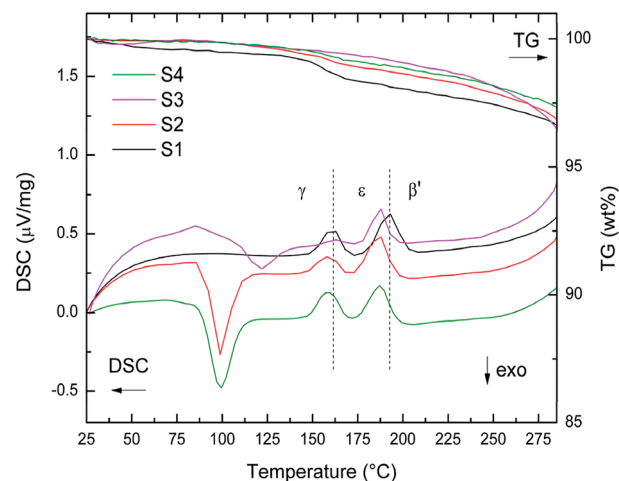

Fig. 3 TG-DSC data of S1–S4 between RT and 285 °C heated at 5 °C min^{-1}. Dashed lines at 153 °C and 185 °C indicate phase transition of as received γ-$Mg(BH_4)_2$ into ε-$Mg(BH_4)_2$ and β'-$Mg(BH_4)_2$.

7 °C min⁻¹) from RT to 450 °C. The average weight loss (Δ*m*) from the TG measurements are given in Table 1 with standard deviations, and compared to the hydrogen contents of the samples. TPD-MS experiments in the range RT – 450 °C (ESI Fig. A5†) show that the mass losses are almost solely due to hydrogen release. Only traces of diborane were detected. The samples lose 80–90% of their hydrogen during the TG-DSC measurements and the relative losses (when accounting for the mass of the additive) are similar within the standard deviations. The TPD-MS experiments also show that the onset of hydrogen release is slightly reduced when comparing S1 to S2–S4, S4 showing the largest reduction.

Isotopic exchange

Isotopic exchange reactions were carried out to study the effect of additives and/or ball milling on the hydrogen sorption kinetics. These measurements were carried out both *ex situ* (long-term exposure) and *in situ* (short-term exposure) for each sample. The samples S1–S4 are re-named S1-D to S4-D after long-term exposure to 3 bar D_2 atmosphere for 23 h at 120 °C. The chosen temperature (120 °C) is above the crystallization temperature of amorphous $Mg(BH_4)_2$ into γ-$Mg(BH_4)_2$ as it was shown earlier that storage or ball milling induces formation of amorphous $Mg(BH_4)_2$.[27] The SR-PXD data at RT of S1-D to S4-D are presented in Fig. 4. The major phase in all samples is porous γ-$Mg(BH_4)_2$. A possible partial substitution of H with D cannot be determined by SR-PXD. Some diffuse scattering is observed, meaning that parts of the samples remain amorphous. In S1-D, a small amount of α-$Mg(BH_4)_2$ (ref. 20) is present (Fig. 4). Since S1 showed very little diffuse scattering, it appears that this α-phase is formed from γ-$Mg(BH_4)_2$. Larger amounts of α-$Mg(BH_4)_2$ are present present in S2-D to S4-D, as well as Bragg peaks of ε-$Mg(BH_4)_2$. The latter is unexpected at RT as the phase transition γ- → ε-$Mg(BH_4)_2$ is observed around 150 °C in TG-

DSC and *in situ* SR-PXD measurements, which is well above the temperature used during the isotopic exchange. Thus, it appears that the transformation occurred at 120 °C, but at too slow a rate to be detected in the heating ramp (SR-PXD and TG-DSC) experiments.

The lack of Bragg peaks from ε-$Mg(BH_4)_2$ in S1-D is possibly due to the slightly higher onset temperature for the γ- → ε-phase transition in the as received sample. A control experiment was conducted (see details in ESI Fig. A6†) and confirms our assumption that the phase transition temperature was not reached. It is worth noting that a previous attempt to preserve ε-$Mg(BH_4)_2$ at RT was unsuccessful, even by rapid quenching.[25] However once it is formed, it is stable on cooling to RT in all our investigated samples.

Spectroscopic studies

Raman and IR spectroscopy are used to identify deuterium substitution in the BH_4 anion. BH_4 has tetrahedral (T_d) symmetry and four normal modes of vibrations. The modes in an isolated T_d molecule are divided into the Raman-active and/ or IR-active as follows: the symmetric stretching and bending modes, ν_1 (A_1) and ν_2 (E) are only Raman-active, while the asymmetric stretching and bending modes, ν_3 (F_2) and ν_4 (F_2) are Raman-active and IR-active. The E mode is doubly degenerate, while the F mode is triply degenerate. It is, however, possible that the inactive mode become active in solids, while the degenerate modes can split due to various solid-state effects.[19] Since D has twice the mass of H, IR and Raman spectroscopy can easily distinguish between stretching and bending modes of B–H and B–D bonds, as they are well separated in energy spectrum.

Fig. 5a and b present IR data at RT for S1 to S4 and for S1-D to S4-D, respectively. In Fig. 5a S1 to S4 show the asymmetric stretching and bending modes ν_3 and ν_4. In good agreement with SR-PXD, our normalized IR data of the ball milled S2–S4 show a slight broadening of ν_3 and ν_4 modes compared to S1, which can be attributed to the amorphization observed in S2–S4. The integrated peak areas of the B–H stretching region are summarized in ESI Table A2† and support the visual inspection: S1 having the smallest area, followed by an increase between 26–30% for the ball milled samples, with tendency S2 < S4 < S3.

After the treatment in deuterium atmosphere, the isotopic exchange is evident in S1-D to S4-D from the appearance of the B–D stretching mode ν_{B-D} at ~1707 cm⁻¹ and the B–D bending region δ_{B-D} at ~965 cm⁻¹ (ν_{B-D} and δ_{B-D} in Fig. 5b). The observed B–D modes are in good agreement with literature.[31,32] S1-D and S2-D have gained the most in intensity in B–D stretching followed by S4-D and S3-D, when comparing the B–H stretching mode ν_3 and combined B–D stretching modes ν_{B-D} after H → D exchange. These observations give a first indication on the extent of exchange after 23 h and imply that the pure materials may have higher exchange rates than those with additives.

It is worth noting, IR data only give a qualitative indication of the isotope exchange, and thus the weight losses measured from TG-DSC measurements (ESI Fig. A3a to A3d†) were used to
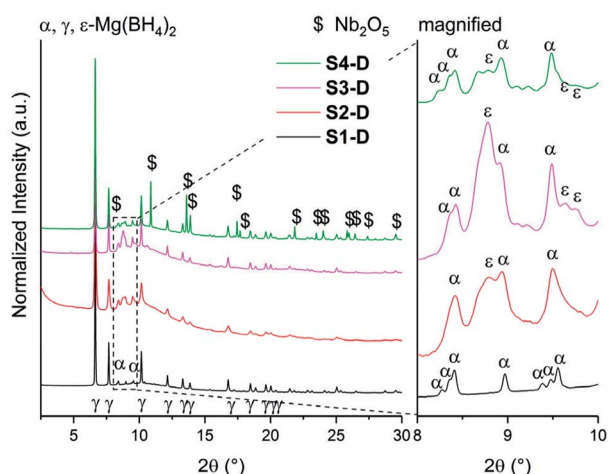

Fig. 4 SR-PXD data of γ-$Mg(BH_4)_2$ samples (S1-D to S4-D) at RT. The samples S1 to S4 were exposed to 3 bar D_2 at 120 °C for 23 h. For comparative reasons, all samples have been normalized to its maximum intensity and are shifted on the *y*-axis for better visibility. Inset showing the magnification of Bragg peaks between $2\theta = 8$–10°. $\lambda = 0.7454$ Å.
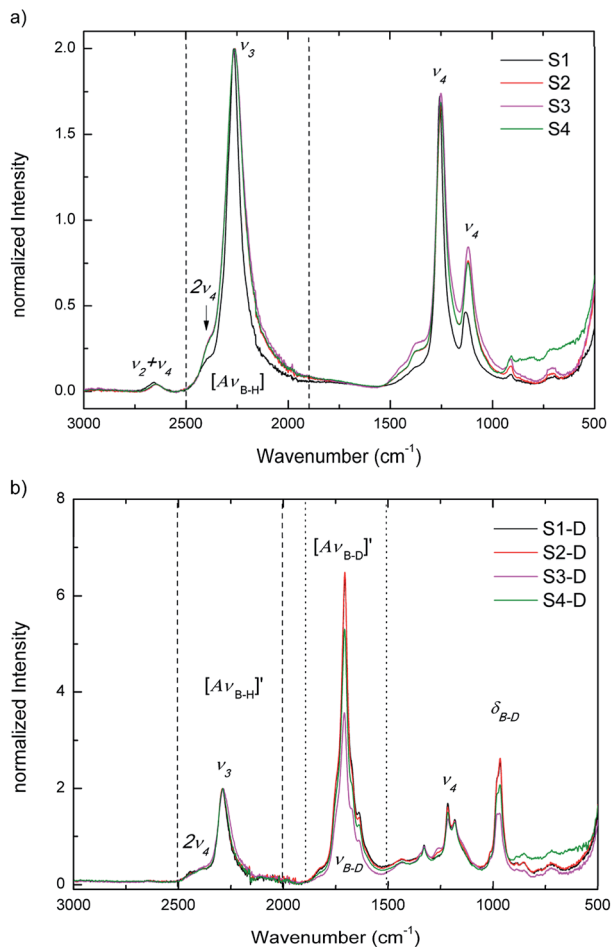
Fig. 5 IR data at RT. (a) of S1–S4; and (b) of S1-D to S4-D after 23 h at 120 °C and 3 bar D_2.

draw quantitative conclusions. The procedure of data treatment is explained in the ESI,† and the results are presented in Table 2 with the actual weight loss compared to masses of D in $Mg(BD_4)_2$. When comparing S1-D, S2-D and S4-D, the deuterium exchanges are similar and within the standard deviations of the measurement, while S3-D has a fairly lower amount of deuterium exchanged. This is in agreement with the IR spectroscopy data after exchange, as the integrated B–D stretching mode ν_{B-D} – area is the lowest among all samples. Furthermore, S3–D shows the largest fraction of the dense polymorphs α- and ε-$Mg(BH_4)_2$ from SR-PXD (visual inspection) and also an increased crystallization temperature from the TG-DSC data.

Table 2 Deuterium content of all samples compared to $Mg(BD_4)_2$, and average weight loss of independent TG-DSC measurements and calculated deuterium content "x" in $Mg(BH_{4-x}D_x)_2$ after 23 h in 3 bar D_2

#	D content (wt%) in $Mg(BD_4)_2$	ΔTG data (wt%)	x in $Mg(BH_{4-x}D_x)_2$
S1-D	26.0	19.0 ± 0.2	1.4 ± 0.1
S2-D	26.0	19.5 ± 0.6	1.5 ± 0.2
S3-D	24.5	16.7 ± 0.2	1.0 ± 0.1
S4-D	24.0	17.2 ± 0.4	1.3 ± 0.1

Thus, these data support the hypothesis of lower hydrogen–deuterium exchange in S3-D.

In situ Raman spectroscopy and adsorption studies

In situ Raman measurements were carried out in order to understand the reaction pathway during the isotopic exchange. In contrast to the isotope exchange investigated by IR, the timescale of these measurements is rather short, 75 min, and thus it is expected that the processes on the surface, dominate the exchange process.

The first set of the in situ Raman experiments were carried out using samples S1 and S2. Fig. 6 shows the in situ Raman data of S1 heated from RT to 175 °C at 2 °C min⁻¹ under 3 bar D_2. Initially, the symmetric stretching (ν_1) and bending (ν_2) modes of the BH_4 anion are observed at 2318 and 1400 cm⁻¹, respectively. Furthermore, the asymmetric BH_4 stretching and bending modes ν_3 and $2\nu_4$ are observed at 2280 and 2208 cm⁻¹. The isotopic exchange seems to start at 81 °C as a new peak appears at 1718 cm⁻¹ and corresponding to the reported region of symmetric B–D stretching (ν_{B-D}).[43] This characteristic peak for B–D stretching is observed at a lower temperature than that reported by Zavorotynska et al.[31] As previously reported,[31] this observation is supported by a decrease in $2\nu_4$ and red shift in ν_1. The latter observation can be explained by the fact that the peak at ~2318 cm⁻¹ actually consists of several overlapping peaks, and is dominated by ν_1 in pure $Mg(BH_4)_2$. Upon deuterium substitution new modes corresponding to the B–H stretching of various $BH_{4-x}D_x$ ions appear causing the apparent broadening and the red shift.

Under the same conditions, no new peak around 1718 cm⁻¹, no decrease in $2\nu_4$ nor shift in ν_1 was observed for sample S2 (ESI Fig. A7a†). This clearly indicates that no H → D exchange takes place in the ball milled sample within the time scale of the measurement. ~38% of the hydrogen was exchanged with deuterium for the sample S2-D during the 23 h exposure described above. However, during the in situ Raman measurements the time where the isotopic exchange can occur (between ~80 and ~150 °C) was only ~35 min. Amorphous $Mg(BH_4)_2$ which is the major component in S2 is not porous as a BET area of only 30 m² g⁻¹ was measured (compared to 900 m² g⁻¹ for γ-$Mg(BH_4)_2$), see Fig. 7 and ESI† Part B – BET area. Therefore, it is predicted to behave like a dense polymorph, relying on slow, long-range bulk diffusion to achieve appreciable isotopic exchange.[32]

The N_2 adsorption–desorption isotherms measured at −196 °C (77 K) are presented in Fig. 7 and Table 3 (more details can be found in the ESI Fig. B1–B4†). The isotherm for S1 is of type I(a) (IUPAC classification[38]), showing a clear plateau region without any signs of hysteresis and highlighting the ultra-microporous character of this material. The calculated BET area is 900 m² g⁻¹. Unlike S1, sample S2 (the ball-milled version of S1) revealed very small BET area (30 m² g⁻¹) and gave a type II isotherm.[38] This is typical for adsorption on non-porous solids, and showing clearly that ball-milling leads to amorphization and to collapse of the porous network (compare SR-PXD in Fig. 1, red curve). However, for comparison the samples S1 and
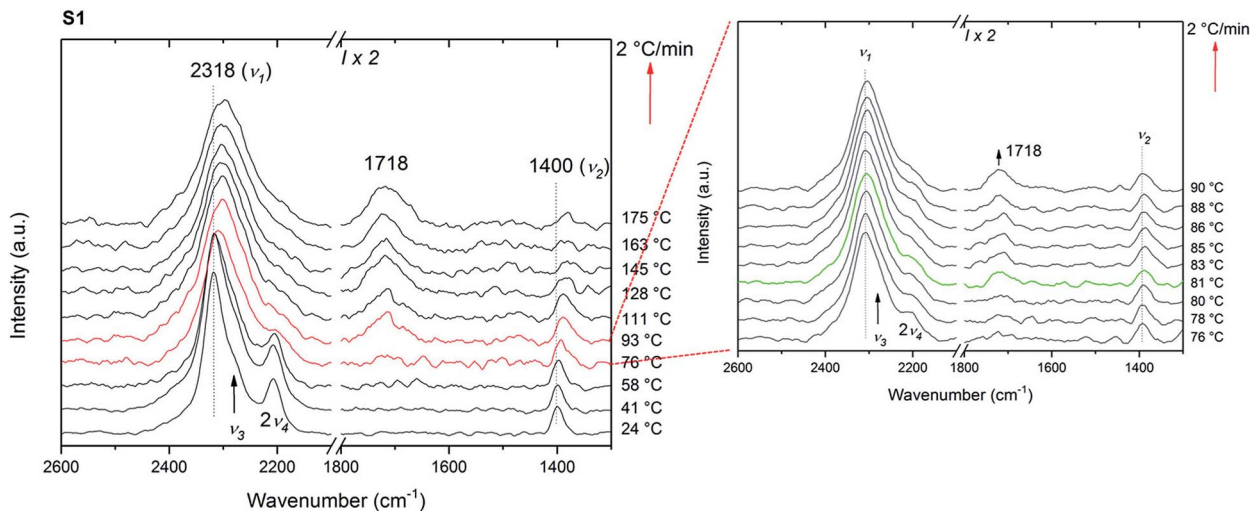
Fig. 6 *In situ* Raman data of S1 including the heating from RT to 175 °C by 2 °C min^{-1} under 3 bar D$_2$. Every 10th measurement is shown except for the inset, where every measurement is presented from 76 to 90 °C. Inset displays the B–D stretching at 81 °C (green curve). All data is translated in *y* axis for clarity.

S2 have been heat treated under hydrogen (120 °C, 23 h, 3 bar H$_2$, sample named SX-H in analogy to SX-D, X = 1, 2). N$_2$ adsorption measurements gave again an ultra-microporous isotherm shape in S1-H and S2-H and a BET area value of 560 m^2 g^{-1} for the latter which is 62% of the BET area of the as received S1 sample (900 m^2 g^{-1}). This suggests that at least part of the porous structure has been regenerated in S2-H. The same is proposed for S2-D and supported by the SR-PXD results shown in Fig. 4 (red curve).

It is shown that the adsorption studies reveal that it is possible to partially regain the porous structure from amorphous Mg(BH$_4$)$_2$ by annealing under hydrogen or deuterium. In combination with the long reaction times allowing for the reaction to approach equilibrium, this explains why the isotope exchange during long term D$_2$ exposure was possible in initially partially amorphous ball-milled samples. Furthermore, part of the porous structure in S1-D collapses under heat treatment (BET area = 690 m^2 g^{-1}), resulting in a BET similar to the other samples and thus to a comparable extent of isotopic exchange in S1-D and S2-D.

In situ Raman data of S3 and S4 are not presented, as the signal-to-noise ratio over the whole spectrum was too low.

Room temperature isotopic exchange

Fig. 8 presents the IR data of S1–S4 after 6 days under 3 bar D$_2$ at RT. Even though with low intensities, B–D stretching is observed for all samples (S1–S4). The normalized IR data of the ball milled S2–S4 show broadening of the stretching and bending modes compared to S1 due to the increased disorder in the local structure of BH$_4^-$ in these largely amorphous samples. To the best of our knowledge, this is the first time that the isotopic exchange reaction was observed at RT under this low pressure of D$_2$ (3 bar) in stable (alkali- and alkaline-earth) borohydrides.
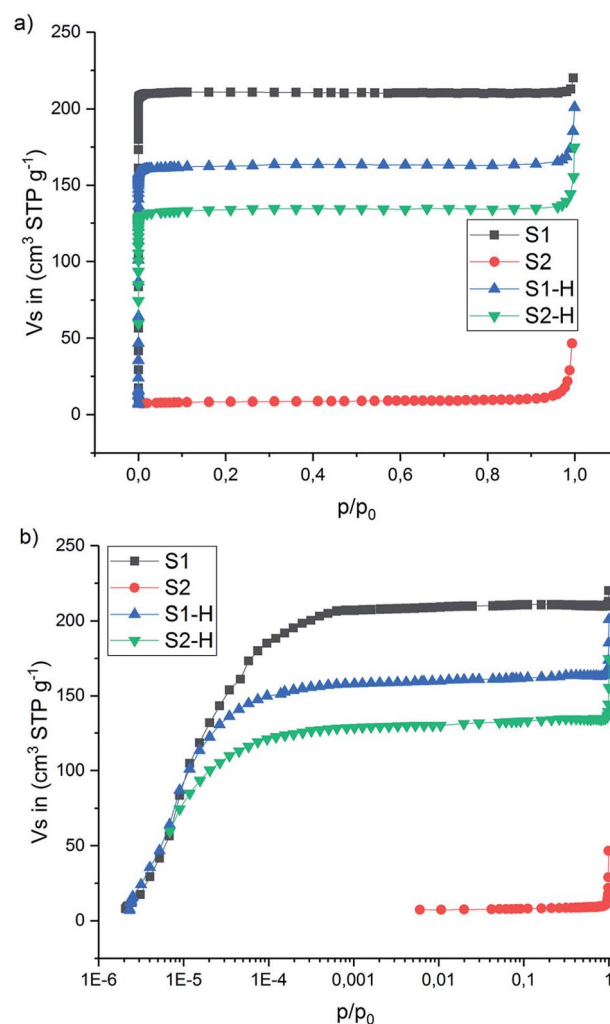

Fig. 7 N$_2$ adsorption–desorption isotherms (77 K) of the S1, S2 and thermally treated S1-H, S2-H. (a) *x*-axis in p/p_0 and (b) *x*-axis in log scale p/p_0.

Table 3 BET, Langmuir, DR and MP areas and total pore volumes

	S1	S1-H	S2	S2-H
BET ($m^2 g^{-1}$)	900	690	30	560
Langmuir ($m^2 g^{-1}$)	915	700	36	570
DR ($m^2 g^{-1}$)	915	700	38	570
MP ($m^2 g^{-1}$)	880	670	29	560
Total pore volume ($cm^3 g^{-1}$)	0.33	0.25	—	0.20
% Surface area (N_2)	100	76	4	62
% Pore volume (N_2)	100	76	—	61
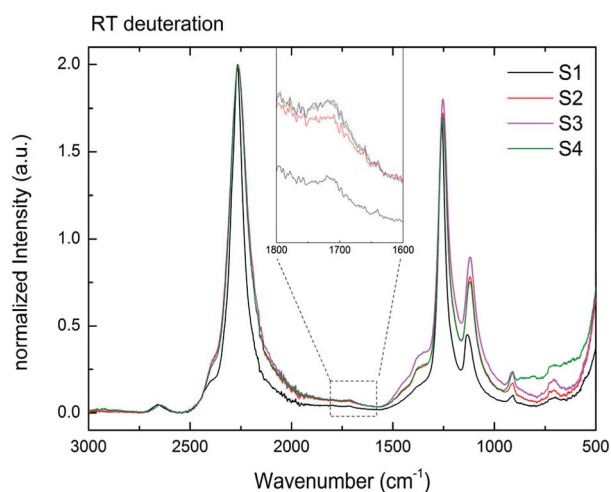
Fig. 8 RT H → D exchange of samples S1–S4 for six days under 3 bar D2. Inset showing a magnification of 1800–1600 cm^{-1}. The B–D stretching mode formed in all samples at RT.

The isotopic exchange at RT was observed for both amorphous (S2–S4) and crystalline (S1) samples. Furthermore, the similar intensities of the B–D stretching in all samples suggest also the similar amounts of the exchanged hydrogen. As shown by the BET measurements for S2 (Table 3), the amorphous $Mg(BH_4)_2$ has a very low surface area and a non-porous structure. Therefore, the H–D exchange observed should be explained mostly by the long-range diffusion of deuterium into the bulk. It can be suggested then that at the long reaction times the equilibrium (at a given temperature) H/D ratio was achieved in both high and low surface $Mg(BH_4)_2$ samples. Indeed, it was shown before for $LiBH_4$ that the amount of the substituted D and the D distribution between the five possible $BH_{4-n}D_n$ units is comparable with the Boltzmann statistical distribution at a given temperature calculated from the zero-point vibrational energy difference between the $BH_{4-n}D_n$ units.[44]

Conclusions

The effect of additives, such as Ni_3B and Nb_2O_5, and the effect of ball milling porous γ-$Mg(BH_4)_2$ have been investigated with respect to both, dehydrogenation and H → D exchange. The additives and the milling process seem to influence the porous γ-phase and slightly lower the phase transition temperature. From TPD-MS it was observed that the hydrogen release temperature

decreased most for the Nb_2O_5 containing sample and the decomposition pathway is altered, yet not completely understood.

The isotopic exchange reactions have shown that neither the milling process nor the additives enhance the solid-state deuterium diffusion reaction in 23 h treated samples. The TG data show that as-received, ball milled and $Mg(BH_4)_2$ with Nb_2O_5 have an H → D exchange between 32 and 37% during the extended treatment in 3 bar deuterium atmosphere, while ball milled $Mg(BH_4)_2$ with Ni_3B only shows 25% isotope exchange.

The *in situ* Raman measurements have shown that the isotopic exchange reaction in as-received γ-$Mg(BH_4)_2$ started at temperatures of ~80 °C under 3 bar of D_2, and thus almost 20 °C lower than reported before. Furthermore, the comparison of the results of *in situ* deuteration observed by the Raman measurements and the *ex situ* deuteration analyzed by the FTIR spectroscopy indicated that the gas–solid H(D) exchange is not the rate-limiting step in the H–D exchange reactions. The concentration of the BD species on the surface of the dense phases was simply too small to be detected by the short Raman measurements. On the other hand, an appreciable exchange in as-received $Mg(BH_4)_2$ with a high BET area (900 $m^2 g^{-1}$) was observable. Similar amount of exchanged D was observed after the long exchange reactions (23 h & 6 days) due to the fact that the long reaction times allowed for the solid-state D diffusion in the bulk of the (partially) amorphous phases.

Finally, IR results show that if all samples are kept for 6 days at 3 bar D_2 the H → D exchange reaction takes place even at RT. To the best of our knowledge, this is the first time that an isotopic exchange reaction has been observed in stable (alkali- and alkaline-earth) boron-based complex metal hydrides at room temperature, indicating that the B–H bonds in $Mg(BH_4)_2$ can be challenged at mild conditions.

Conflicts of interest

There are no conflicts to declare.

Acknowledgements

References

1 B. Bogdanović and M. Schwickardi, *J. Alloys Compd.*, 1997, **253**, 1.

2 M. J. v. Setten, G. A. d. Wijs, M. Fichtner and G. Brocks, *Chem. Mater.*, 2008, **20**, 4952.

3 V. Ozolins, E. Majzoub and C. Wolverton, *Phys. Rev. Lett.*, 2008, **100**, 135501.

4 G. Severa, E. Rönnebro and C. M. Jensen, *Chem. Commun.*, 2010, **46**, 421.

5 M. Chong, A. Karkamkar, T. Autrey, S.-i. Orimo, S. Jalisatgi and C. M. Jensen, *Chem. Commun.*, 2011, **47**, 1330.

6 O. Zavorotynska, S. Deledda and B. C. Hauback, *Int. J. Hydrogen Energy*, 2016, **41**, 9885.

7 E. G. Bardají, N. Hanada, O. Zabara and M. Fichtner, *Int. J. Hydrogen Energy*, 2011, **36**, 12313.

8 A. Al–Kukhun, H. T. Hwang and A. Varma, *Int. J. Hydrogen Energy*, 2012, **37**, 17671.

9 H.-W. Li, K. Kikuchi, Y. Nakamori, K. Miwa, S. Towata and S. Orimo, *Scr. Mater.*, 2007, **57**, 679.

10 I. Saldan, C. Frommen, I. Llamas-Jansa, G. Kalantzopoulos, S. Hino, B. Arstad, R. Heyn, O. Zavorotynska, S. Deledda, M. Sørby, H. Fjellvåg and B. C. Hauback, *Int. J. Hydrogen Energy*, 2015, **40**, 12286.

11 D. Matsumura, T. Ohyama, Y. Okajima, Y. Nishihata, H.-W. Li and S.-i. Orimo, *Mater. Trans.*, 2011, **52**, 635.

12 Z. Zhang, H. Wang, J.-W. Liu and M. Zhu, *Thermochim. Acta*, 2013, **560**, 82.

13 O. Zavorotynska, I. Saldan, S. Hino, T. Humphries, S. Deledda and B. Hauback, *J. Mater. Chem. A*, 2015, **3**, 6592.

14 O. Zavorotynska, S. Deledda, J. G. Vitillo, I. Saldan, M. N. Guzik, M. Baricco, J. C. Walmsley, J. Muller and B. C. Hauback, *Energies*, 2015, **8**, 9173.

15 J. Chen, Y. Zhang, Z. Xiong, G. Wu, H. Chu, T. He and P. Chen, *Int. J. Hydrogen Energy*, 2012, **37**, 12425.

16 E. Albanese, G. N. Kalantzopoulos, J. Vitillo, E. Pinatel, B. Civalleri, S. Deledda, S. Bordiga, B. Hauback and M. Baricco, *J. Alloys Compd.*, 2013, **580**, S282.

17 G. Kalantzopoulos, J. Vitillo, E. Albanese, E. Pinatel, B. Civalleri, S. Deledda, S. Bordiga, M. Baricco and B. Hauback, *J. Alloys Compd.*, 2014, **615**, S702.

18 I. Saldan, S. Hino, T. D. Humphries, O. Zavorotynska, M. Chong, C. M. Jensen, S. Deledda and B. C. Hauback, *J. Phys. Chem. C*, 2014, **118**, 23376.

19 O. Zavorotynska, A. El-Kharbachi, S. Deledda and B. C. Hauback, *Int. J. Hydrogen Energy*, 2016, **41**, 14387.

20 Y. Filinchuk, R. Černý and H. Hagemann, *Chem. Mat.*, 2009, **21**, 925.

21 J.-H. Her, P. W. Stephens, Y. Gao, G. L. Soloveichik, J. Rijssenbeek, M. Andrus and J.-C. Zhao, *Acta Crystallogr., Sect. B: Struct. Sci.*, 2007, **63**, 561.

22 Y. Filinchuk, B. Richter, T. R. Jensen, V. Dmitriev, D. Chernyshov and H. Hagemann, *Angew. Chem., Int. Ed.*, 2011, **50**, 11162.

23 B. Richter, D. B. Ravnsbæk, N. Tumanov, Y. Filinchuk and T. R. Jensen, *Dalton Trans.*, 2015, **44**, 3988.

24 W. David, S. Callear, M. Jones, P. Aeberhard, S. Culligan, A. Pohl, S. Johnson, K. Ryan, J. Parker and P. Edwards, *Phys. Chem. Chem. Phys.*, 2012, **14**, 11800.

25 M. Paskevicius, M. P. Pitt, C. J. Webb, D. A. Sheppard, U. Filsø, E. M. Gray and C. E. Buckley, *J. Phys. Chem. C*, 2012, **116**, 15231.

26 C. Pistidda, S. Garroni, F. Dolci, E. G. Bardaji, A. Khandelwal, P. Nolis, M. Dornheim, R. Gosalawit, T. Jensen, Y. Cerenius, S. Surinach, M. D. Baro, W. Lohstroh and M. Fichtner, *J. Alloys Compd.*, 2010, **508**, 212.

27 V. Ban, A. V. Soloninin, A. V. Skripov, J. Hadermann, A. Abakumov and Y. Filinchuk, *J. Phys. Chem. C*, 2014, **118**, 23402.

28 G. N. Kalantzopoulos, M. K. Antoniou, A. Enotiadis, K. Dimos, E. Maccallini, A. Policicchio, E. Colavita and R. G. Agostino, *J. Mater. Chem. A*, 2016, **4**, 9275.

29 G. N. Kalantzopoulos, A. Enotiadis, E. Maccallini, M. Antoniou, K. Dimos, A. Policicchio, E. Klontzas, E. Tylianakis, V. Binas, P. N. Trikalitis, R. G. Agostino, D. Gournis and G. E. Froudakis, *Int. J. Hydrogen Energy*, 2014, **39**, 2104.

30 M. Sharma, D. Sethio, V. D'Anna, J. C. Fallas, P. Schouwink, R. Černý and H. Hagemann, *J. Phys. Chem. C*, 2015, **119**, 29.

31 O. Zavorotynska, S. Deledda, G. Li, M. Matsuo, S. i. Orimo and B. C. Hauback, *Angew. Chem.*, 2015, **127**, 10738.

32 H. Hagemann, V. D'Anna, J.-P. Rapin and K. Yvon, *J. Phys. Chem. C*, 2010, **114**, 10045.

33 G. Barkhordarian, T. Klassen and R. Bormann, *Scr. Mater.*, 2003, **49**, 213.

34 M. Wojdyr, *J. Appl. Crystallogr.*, 2010, **43**, 1126.

35 H. Brinks, A. Fossdal, R. Bowman and B. C. Hauback, *J. Alloys Compd.*, 2006, **417**, 92.

36 A. Hammersley, *FIT2D: An introduction and overview*, ESRF Int. Rep., ESRF97HA02T, 1997.

37 V. Dyadkin, P. Pattison, V. Dmitriev and D. Chernyshov, *J. Synchrotron Radiat.*, 2016, **23**, 825.

38 M. Thommes, K. Kaneko, A. V. Neimark, J. P. Olivier, F. Rodriguez-Reinoso, J. Rouquerol and K. S. Sing, *Pure Appl. Chem.*, 2015, **87**, 1051.

39 M. M. Dubinin, *J. Colloid Interface Sci.*, 1974, **46**, 351.

40 M. M. Dubinin and L. Radushkevich, *Chem. Zentralbl.*, 1947, **1**, 875.

41 W. I. F. David, S. K. Callear, M. O. Jones, P. C. Aeberhard, S. D. Culligan, A. H. Pohl, S. R. Johnson, K. R. Ryan, J. E. Parker, P. P. Edwards, C. J. Nuttall and A. Amieiro-Fonseca, *Phys. Chem. Chem. Phys.*, 2012, **14**, 11800.

42 S. Guo, H. Y. L. Chan, D. Reed and D. Book, *J. Alloys Compd.*, 2013, **580**, S296.

43 G. Renaudin, S. Gomes, H. Hagemann, L. Keller and K. Yvon, *J. Alloys Compd.*, 2004, **375**, 98.

44 R. Gremaud, Z. Łodziana, P. Hug, B. Willenberg, A. M. Racu, J. Schoenes, A. J. Ramirez-Cuesta, S. J. Clark, K. Refson, A. Züttel and A. Borgschulte, *Phys. Rev. B: Condens. Matter Mater. Phys.*, 2009, **80**, 100301.